Observation of Hydrodynamic Flows in Imploding Fusion Plasmas on the National Ignition Facility

D. J. Schlossberg,[1,*] G. P. Grim,[1] D. T. Casey,[1] A. S. Moore,[1] R. Nora,[1] B. Bachmann,[1] L. R. Benedetti,[1] R. M. Bionta,[1] M. J. Eckart,[1] J. E. Field,[1] D. N. Fittinghoff,[1] M. Gatu Johnson,[2] V. Geppert-Kleinrath,[3] E. P. Hartouni,[1] R. Hatarik,[1] W. W. Hsing,[1] L. C. Jarrott,[1] S. F. Khan,[1] J. D. Kilkenny,[4] O. L. Landen,[1] B. J. MacGowan,[1] A. J. Mackinnon,[1] K. D. Meaney,[3] D. H. Munro,[1] S. R. Nagel,[1] A. Pak,[1] P. K. Patel,[1] B. K. Spears,[1] P. L. Volegov,[3] and C. V. Young[1]

[1]*Lawrence Livermore National Laboratory, Livermore, California 94550, USA*
[2]*Massachusetts Institute of Technology Plasma Science and Fusion Center, Cambridge, Massachusetts 02139, USA*
[3]*Los Alamos National Laboratory, Los Alamos, New Mexico 87544, USA*
[4]*General Atomics, La Jolla, California 92121, USA*

(Received 11 March 2020; revised 6 June 2021; accepted 8 July 2021; published 13 September 2021)

Inertial confinement fusion implosions designed to have minimal fluid motion at peak compression often show significant linear flows in the laboratory, attributable per simulations to percent-level imbalances in the laser drive illumination symmetry. We present experimental results which intentionally varied the mode 1 drive imbalance by up to 4% to test hydrodynamic predictions of flows and the resultant imploded core asymmetries and performance, as measured by a combination of DT neutron spectroscopy and high-resolution x-ray core imaging. Neutron yields decrease by up to 50%, and anisotropic neutron Doppler broadening increases by 20%, in agreement with simulations. Furthermore, a tracer jet from the capsule fill-tube perturbation that is entrained by the hot-spot flow confirms the average flow speeds deduced from neutron spectroscopy.

DOI: 10.1103/PhysRevLett.127.125001

Inertial confinement fusion relies on balanced compression of a target to areal densities large enough to confine a burning, thermonuclear plasma [1]. During indirect-drive inertial confinement fusion (ICF), lasers focused on the inner walls of a high-Z cavity convert laser energy into thermal x rays. These x rays then impinge on a spherical target within the cavity, ablating its outer layer and driving the implosion. Uniformity in compression is critical for achieving high performance and coupling the maximum amount of energy into the implosion.

However, implosions are generally observed to have low-mode, volumetric asymmetries that are hypothesized to be due to laser drive asymmetry [2–6] and center-of-mass motion [7,8] of the fusing plasma ("hot spot"). These asymmetries degrade performance through several channels, including increased conduction losses [9], radiative losses [10,11], and residual kinetic energy left unconverted to thermal energy [12]. At the National Ignition Facility (NIF), recent implosions with the largest performance discrepancy between 2D predictions and experiment are seen to have large mode 1 asymmetries [13,14] in the shell areal density and hot-spot velocity.

In this Letter, we report results from systematically manipulating radiation-drive asymmetry to evaluate effects on implosion performance. To isolate effects from asymmetric drive, we kept the capsule, fuel, high-Z cavity, laser pulse shape, and total power constant and varied the balance of laser energy entering each end of the cavity. Larger laser imbalance produces stronger capsule-drive asymmetry. As this drive asymmetry increases, we find increased hot-spot drift velocity (v_{HS}), degraded neutron yield, broadened neutron energy spectra, limb brightening in x-ray images, and stronger vortical flow fields internal to the fusing plasma. These degradations directly inform ignition-type implosions. Results agree with trends in recent theoretical work [15–17], which provides a framework for interpreting effects of fuel velocity variance on observed neutron energy spectra. Two-dimensional, hydrodynamic simulations agree with trends, though discrepancies exist in absolute parameter values. The dominant flow within the hot spot is directly imaged through a tracer reaching >200 km/s through deuterium-tritium (DT) plasmas of density >10 g/cm^3 and pressures >10 Gbar. These flows imply a significant fraction of the radiation drive remains as residual kinetic energy. The measured, time-resolved fluid motion tracks predicted paths and has comparable magnitudes to simulated values. This work presents a consistent understanding across experiment, simulation, and theory of the effect of low-mode drive asymmetries on ICF implosions.

Figure 1 depicts experimental details of this set of implosions. The target comprised a 5.4-mm-diameter by 10.13-mm-tall gold cavity ("hohlraum") [Fig. 1(a)], inside which was suspended a hollow capsule with a 64-μm-thick

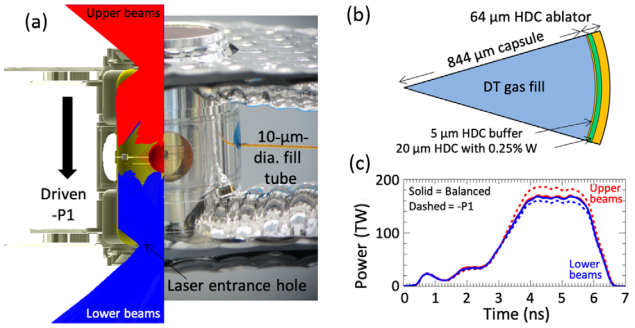

FIG. 1. (a) Hohlraum model and photo, with example $P1$ drive; (b) SymCap constituents; (c) example laser drive waveforms.

high-density carbon (HDC) ablator shell [Fig. 1(b)]. A 25-μm-thick portion of this shell was doped with 0.25% tungsten, shown to improve performance [18,19]. Gaseous DT fuel was fed into the capsule before each implosion via a 10-μm-diameter fill tube, shown in Fig. 1(a). Using gaseous DT fuel with added mass-equivalent ablator as surrogates for an ignition-type DT-ice layer has successfully tuned symmetry of capsules [6,20], with accurate scaling to ignition-relevant targets. Here, targets were cooled to 32 K to achieve the required hohlraum ^{4}He fill density (0.3 mg/cm^3) and DT fuel density ($\sim$4 mg/cm^3). The gold hohlraum walls were then illuminated with a 1.1 MJ, 340 TW peak-power laser pulse shown in Fig. 1(c). The pulse shape matched the high-performance, high-adiabat "Bigfoot" pulse [20,21]. Simulations show 94% of the HDC shell was ablated. Average energy was kept sufficiently constant from shot to shot, with total energy in the peak reproducible to $\pm$0.8% across all cases. X-ray drive asymmetries were induced only by altering the balance of upper and lower NIF outer cone power during the peak drive, with a maximum of $\pm$8%. An example asymmetric pulse is shown in Fig. 1(c) as dashed lines and corresponds to the driven $-P1$ direction shown in Fig. 1(a).

Nuclear results from the implosion with the largest drive asymmetry are shown in Fig. 2. Locations are given in spherical coordinates, with $\theta = 0°$ (vertical) aligned with Fig. 1(a)'s hohlraum axis and ϕ around the hohlraum's azimuth. Neutron time-of-flight diagnostics (NTOF) [22] at four locations measure the neutron spectrum along a line of sight (LOS) by determining its arrival time from the effectively instantaneous emission ($\sim$0.1 ns). By taking moments of this spectrum with respect to time, we derived the neutron yield [23], bulk hot-spot velocity [24] and apparent ion temperature, T_{ion} [25–27]. Measured values for these quantities are shown next to each LOS. These four LOS velocities were used to solve for three hot-spot velocity components (v_x, v_y, v_z) plus an isotropic component due to the reactants' thermal energy. The resulting hot-spot drift velocity for this case corresponds to a magnitude and direction of 121 $\pm$ 15 km/s toward (177°, 171°).

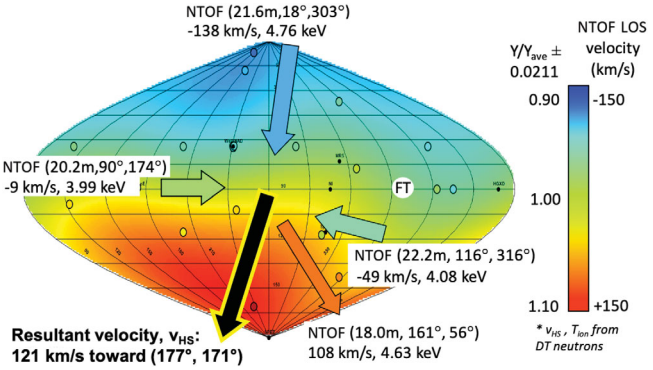

FIG. 2. NTOF velocities along four lines of sight, overlaid on a neutron activation sky map; lines of latitude (longitude) are on 15° (30°) intervals and centered at 90° (270°). "FT" denotes the fill-tube location, and the $-P1/P0$ case shown is shot N171022-001.

Independent confirmation of this velocity is provided by flange neutron activation detectors, comprising 24 zirconium samples distributed around the target chamber [28,29]. Since the $^{90}\mathrm{Zr}(n,2n)^{89}\mathrm{Zr}$ activation cross section increases with energy [28,30], any energy increase given to the 14.028-MeV DT neutrons from the reactants' center-of-mass velocity will produce higher activation in the direction of that velocity. A spherical-harmonic expansion has been fit to the activation data from each Zr detector and is shown in Fig. 2 as an underlaid color map. The peak activation (red) tightly correlates with the resultant v_{HS} derived from NTOF measurements. Furthermore, this activation difference arises from velocity effects and not from areal density [31], as expected for this gas-filled implosion with fuel and shell areal densities of only $\sim$0.1 and 0.4 g/cm^2, respectively. These independent measures of v_{HS} were consistent across all implosions in this series. The agreement across multiple, independent diagnostics provides confidence that observed velocities are indeed produced by the imposed laser asymmetry.

Drive-asymmetry signatures in x-ray [32,33] and neutron imaging [34–36] are shown in Fig. 3. Time-integrated $\lesssim$8 keV x-ray imaging is presented along two sight lines: the top row looking from (090°, 100°) and the bottom row from (090°, 315°). The imposed drive asymmetries vary from $-P1/P0$ to nominally balanced to $+P1/P0$. v_{HS} vectors (white arrows) are projected into each image's LOS. Here, $P1/P0$ is defined as the Legendre decomposition of drive into its first mode $P1$ and normalized to the 0th mode $P0$ [37].

The top row in Fig. 3 shows that this velocity correlates with shell limb brightening in all cases, which is indicative of hot fuel depositing energy in the remaining HDC [38]. The bottom row in Fig. 3 overlays neutron production contours onto collocated x-ray images. Note that the "streak" present in all images is due to high-Z dopant entrained by a fill-tube-induced jet, as will be discussed below, and was not included in the 2D simulations presented herein.

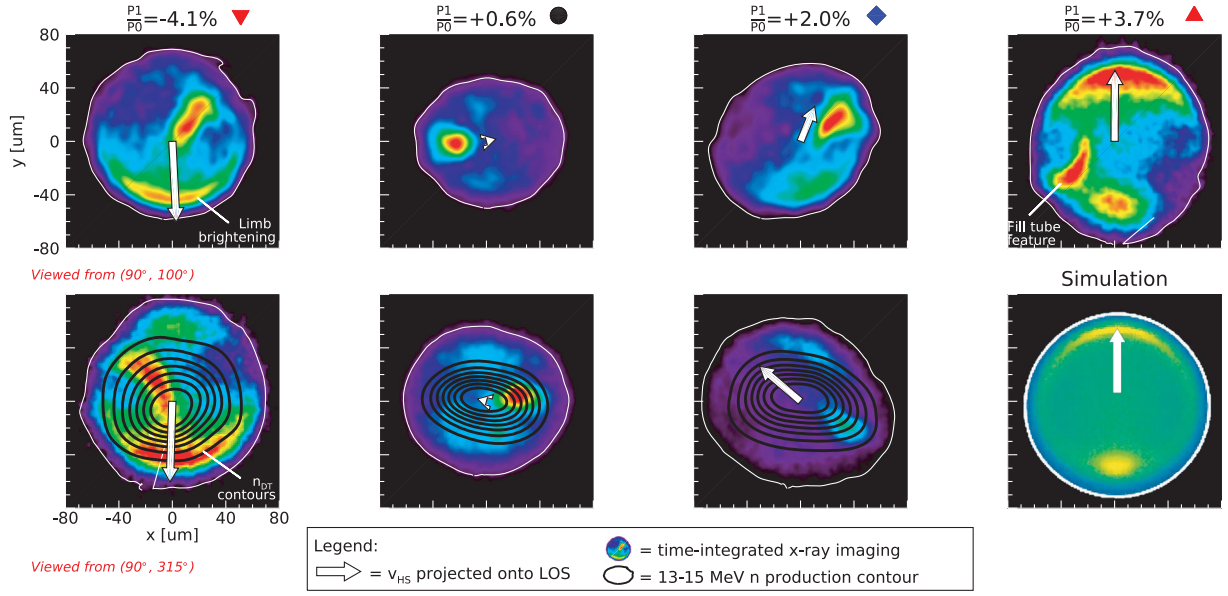

FIG. 3. NTOF bulk velocities (white arrows) are consistent with features inside the hot spot. Top row: The x-ray limb brightening and fill-tube streak are correlated with v_{HS}. Bottom row: overlaid 13–15 MeV n production contours, evenly spaced from 17% to 95%. From left to right, v_{HS}: $(121 \pm 15$ km/s, $177 \pm 14°$, $171 \pm 168°)$; $(78 \pm 20$ km/s, $24 \pm 22°$, $243 \pm 43°)$; $(15 \pm 22$ km/s, $95 \pm 70°$, $155 \pm 89°)$; $(118 \pm 16$ km/s, $8 \pm 12°$, $356 \pm 95°)$.

The far-right column in Fig. 3 compares measured x-ray imaging with a synthetic x-ray image from 2D HYDRA modeling [39], both with similar drive asymmetry. In both images, two distinct features are observed: increased x-ray emission in the direction of v_{HS} (white arrow) and also diametrically opposite. Note that the fill tube was not included in these simulations. X-ray emission is proportional to n and T, and simulations have suggested that fluid motion within the hot spot can lead to increased temperature parallel to v_{HS} and increased density antiparallel to v_{HS} (see Fig. 3 in Ref. [5]). New simulations, shown below and in Supplemental Material [40], suggest that fuel at the north pole is pushed out of the way of this incoming jet, travels around the hot-spot periphery confined by the imploding shell, and stagnates near the south pole. This increased density leads to increased x-ray emission. While not conclusive, observed x-ray images are strikingly similar to those generated by vortical flows in simulations.

Global, burn-averaged quantities also trend similarly between simulation and observation as shown in Fig. 4. A series of 2D HYDRA capsule-only simulations imposed increasing $P1/P0$ drive asymmetries and tallied quantities using synthetic diagnostics along representative lines of sight. Simulation outputs (empty symbols) and experimental measurements (stars) are compared versus $P1/P0$ drive asymmetry. Experimental $P1/P0$ values are estimated from view factor calculations using asymmetries in measured laser delivery and hohlraum structure, including diagnostic windows [41]. Fits to the data are described in Supplemental Material [40]. Simulated $P1/P0$ values trend with observations, though they lie outside experimental uncertainties. As seen, the $P1/P0$ value derived for N171112 is anomalously low given its drift velocity. The batch of ablator capsules from which this shell originated is suspected to have mass differentials in the poles, which serves to increase the measured drift velocity for no increase in applied laser $P1$ [42,43].

Experimentally measured yields decrease more rapidly than simulation [Fig. 4(b)]. However, both fall more slowly than previous simulations of DT-layer, CH capsules driven by a "low-foot" laser pulse [5], suggesting that layered implosions are even more sensitive to $P1/P0$ asymmetries than gas-filled capsules used here.

It has been established that apparent T_{DT} derived from NTOF measurements is increased by the variance in the reacting fuel's velocity distribution [3,16,44]. NTOF views parallel to the induced v_{HS} often see increased velocity variance and, hence, broadened T_{DT}; herein, we distinguish

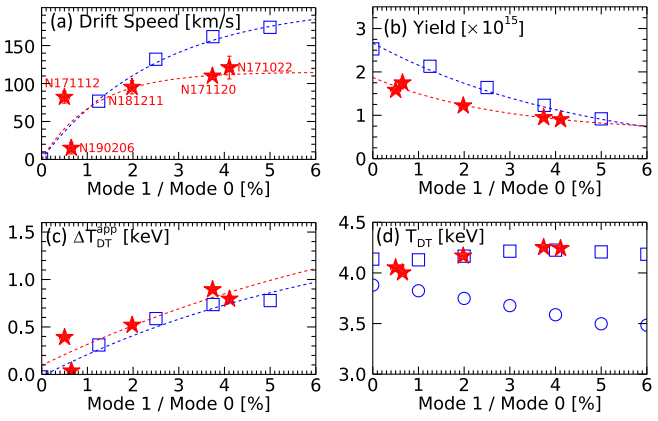

FIG. 4. Measured (stars) and simulated (empty) values versus mode 1 over mode 0 amplitude for (a) v_{HS}, (b) DT-neutron yield,(c) T_{DT}^{app} anisotropy, and (d) T_{DT}^{app} and $T_{DT,thermal}$ (circles).

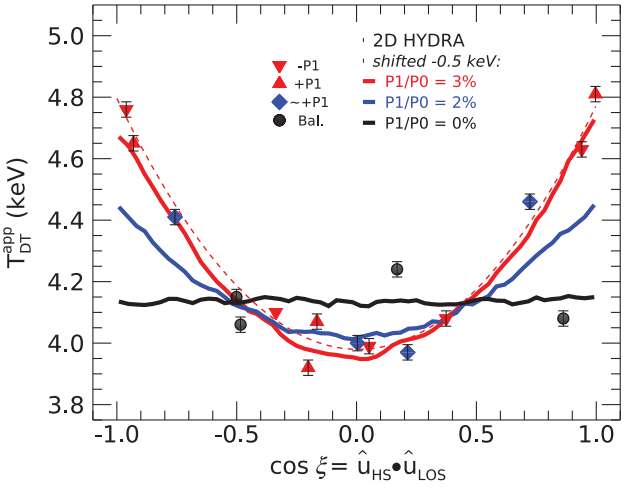

FIG. 5. Apparent T_{ion} versus angle between observer and v_{HS}. Symbols are measured values and their shapes suggest applied asymmetry (i.e., red down pointing triangle for $-P1$). Solid lines are simulations uniformly shifted by -0.5 keV. The dashed red line is theoretical calculation from Eq. (1).

that observable as "apparent T_{DT}" ($T_{\mathrm{DT}}^{\mathrm{app}}$). Figure 4(c) plots the growth in the maximum apparent temperature *difference*, $\Delta T_{\mathrm{DT}}^{\mathrm{app}}$, as observed along different NTOF LOS. We find that, as asymmetric drive increases, the contribution of flow variance to $T_{\mathrm{DT}}^{\mathrm{app}}$ also increases. This trend is confirmed by experiment and simulation. In Fig. 4(d), simulations show that the actual thermal ion temperature decreases as implosions become increasingly perturbed; however, a simple average of the $T_{\mathrm{DT}}^{\mathrm{app}}$ over 4π steradians remains almost constant, since it is broadened by increased flow variance from the induced v_{HS}. This broadening roughly cancels the lost spectral width as thermal T_{DT} decreases and is consistent with the average $T_{\mathrm{DT}}^{\mathrm{app}}$ from measured DT neutron spectra.

To exhibit this velocity variance effect on neutron spectral broadening, in Fig. 5 we plot the measured $T_{\mathrm{DT}}^{\mathrm{app}}$ values from four implosions with varied $P1/P0$ amplitudes versus the cosine of their observation angle ξ. Here, ξ is defined as the angle between the detector LOS and the v_{HS} direction. When $\cos\xi = \pm 1$, the LOS and flow direction are parallel and antiparallel, respectively. Even though v_{HS} changes sign between parallel and antiparallel LOS (e.g., Fig. 2), the velocity *variance* is positive definite and, thus, broadens the observed neutron spectrum equally at angles $\pm\xi$ with respect to v_{HS}. This has been derived mathematically [27]:

$$\mathrm{Var}(\omega) = \langle\tau\rangle + \mathrm{Var}(u_{\parallel}) + \cdots, \tag{1}$$

where ω is the scaled, shifted neutron momentum [15], $\mathrm{Var}(\omega) = \langle\omega^2\rangle - \langle\omega\rangle^2$ is the square of the standard deviation of the observed distribution, $\langle\tau\rangle$ is the mean, or apparent, temperature, and $\mathrm{Var}(u_{\parallel})$ is the variance of the velocity parallel to the observer's line of sight. This theoretical relationship is plotted for the $\pm P1$ case in Fig. 5 (dashed red curve). From this formalism, measurements shown correspond to velocity variances of $(130\ \mathrm{km/s})^2$, $(100\ \mathrm{km/s})^2$, and $(0\ \mathrm{km/s})^2$ for decreasing $P1/P0$ magnitudes.

The results from 2D HYDRA simulations are overlaid in the figure as solid lines. Note that 2D HYDRA overpredicts the absolute ion temperature by roughly 0.5 keV, though it exhibits identical trends as the measurements. Also, in both simulation and data, the minimum $T_{\mathrm{DT}}^{\mathrm{app}}$ decreases with increasing $P1/P0$ magnitude, which implies that the implosion becomes increasingly perturbed and loses more energy to residual kinetic energy.

Figure 5 shows consistency between measurement, simulation, and theory for the effects of a $P1/P0$ perturbation on $T_{\mathrm{DT}}^{\mathrm{app}}$. As $P1/P0$ increases, all three agree that flow variance increases the $T_{\mathrm{DT}}^{\mathrm{app}}$ due to reactants' initial velocities. A direct measurement of the expected flow-variance broadening could be obtained by mapping out reactant velocity streamlines.

We accomplish this by the method shown in Fig. 6(a), which shows a time sequence of x-ray emission images measured perpendicular to the $-P1/P0$ direction [45–47]. A bright emission region originates at the angular location of the fill tube (FT) and traverses the hot spot over time. During an implosion, the fill tube entrains a jet of material ahead of the main shock [48–50], which in these capsules includes a high-Z tungsten dopant. This entrained material emits x rays more strongly than background deuterium or tritium and serves as a tracer particle for flows internal to the hot spot. It is observed in all drive cases in this study.

Figures 6(b) and 6(c) show results of tracking this tracer (centroid of 90% contour) through the hot spot over time [51]. Motion is decomposed into horizontal and vertical velocities and shown for three applied drives. Symbols correspond to the applied perturbation direction: $+P1/P0$ (Δ), balanced ($\circ$), and $-P1/P0$ (∇). Horizontal velocities [Fig. 6(b)] remain negative and approximately constant over time, indicative of radially inward motion with little or no drive perturbation in the horizontal direction. This large horizontal velocity, aligned with an initial fill-tube axis and impervious to drive asymmetry, has been predicted by simulations [48,49] and is unrelated to imposed $P1/P0$. Simulated values at similar times and locations to measurements (hollow triangles) lie within uncertainties.

In contrast, vertical acceleration is clearly observed in imbalanced cases and is correlated with the drive asymmetry direction [Fig. 6(c)]. Observed vertical flow velocities exceed 250 km/s at late times in the most imbalanced cases. Prediction from simulations (hollow green triangles) support internal flows of these magnitudes and directions. This is the first direct observation of hydrodynamic fuel flow during imploding ICF plasmas, with densities and pressures exceeding 10 g/cm^3 and 10 Gbar, respectively. Maximum, instantaneous velocities are larger than NTOF

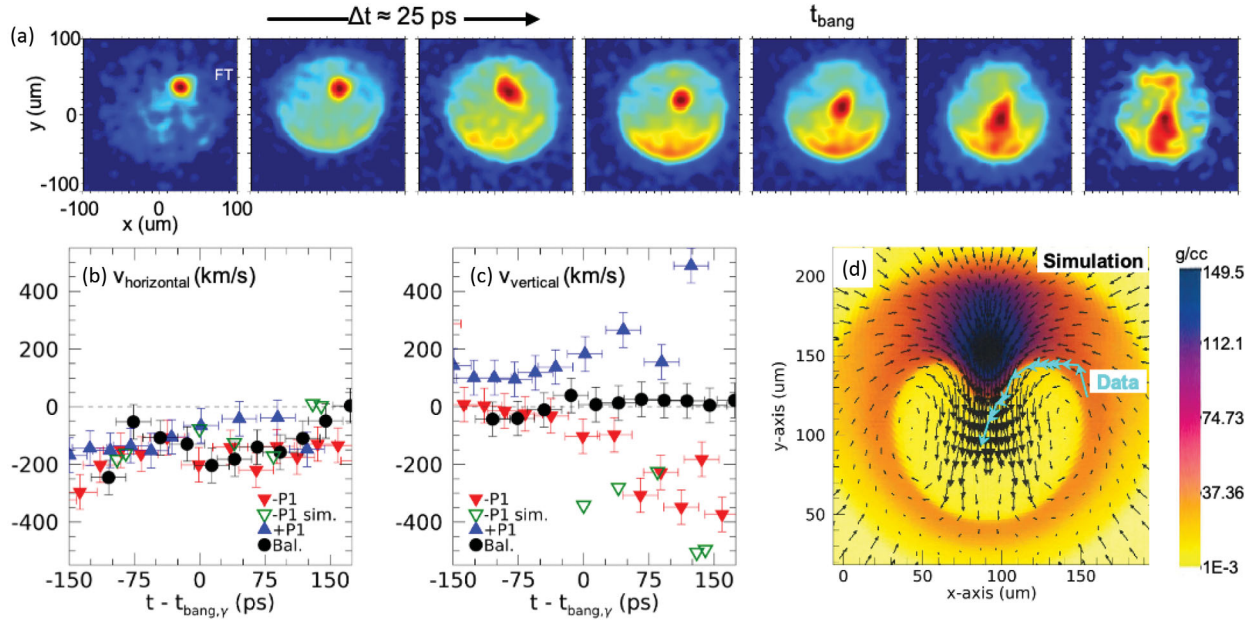

FIG. 6. Measured and simulated flow within imploding ICF hot spots. (a) Time-resolved sequence of measured x-ray emission during a single implosion, viewed orthogonal to imposed asymmetry. (b) Horizontal and (c) vertical flow velocity for three asymmetry drives. (d) Streamline data of internal flows from $-P1/P0$, overlaid on flow field from 2D HYDRA simulation at $t_{\mathrm{bang}} + 65$ ps.

bulk flows (Fig. 3), since measured v_{HS} is necessarily temporally and spatially averaged. As the implosion evolves through peak fusion yield ($t = t_{\mathrm{bang},\gamma}$), the measured v_{HS} is a convolution of the instantaneous velocity field with the neutron production field, at each instant in time. Assuming a Gaussian burn profile of measured duration [52], the convolution for the $-P1/P0$, $+P1/P0$, and balanced implosions shown are -113, 153, and 3 km/s, respectively. Note the $+P1/P0$ case is heavily influenced by the >400 km/s measurement, and excluding that point returns 129 km/s. These burn-averaged velocities are consistent and within uncertainties of measured NTOF v_{HS} above.

An additional consideration lies in flows that counterpropagate around the hot-spot periphery as described above. This motion sets up a vortical flow pattern suggested by previous simulations [4,53] and shown here from 2D HYDRA calculations of these implosions [Fig. 6(d) and Supplemental Material [40]]. The *measured* path during one implosion is overlaid on simulated velocity (arrows) and density (color map) fields. Each point in this path is determined by the tracer's centroid at a given time, and the velocity vector is drawn based on v_{horiz} and v_{vert} at that time. The simulation shown is at $t_{\mathrm{bang}} + 65$ ps, though similar flow behavior is seen throughout. Near the bottom of the shell, the velocity is seen to turn up and outward, implying counterpropagating flows along the hot-spot edge. When observed along a single NTOF LOS, this retrograde motion necessarily contributes to velocity variance and, hence, broadens $T_{\mathrm{DT}}^{\mathrm{app}}$. Lines of sight parallel to the simulated $P1/P0$ will see increased variance while those normal will not, which is consistent with measured $T_{\mathrm{DT}}^{\mathrm{app}}$ values in Fig. 5.

In summary, deleterious effects of asymmetric drive on implosion performance have been quantified. The broadened neutron energy spectra are in agreement with expectation from simulated bidirectional motion of these flows. Time-resolved flows internal to the hot spot are visualized for the first time using a natural tracer jet. Simulations trend similarly to measurements as a function of hot-spot velocity. This work identifies and quantifies a major degradation source relevant for ignition-type targets.

This work was performed under the auspices of the U.S. Department of Energy by Lawrence Livermore National Laboratory under Contract No. DE-AC52-07NA27344. This document was prepared as an account of work sponsored by an agency of the United States government. Neither the United States government nor Lawrence Livermore National Security, LLC, nor any of their employees makes any warranty, expressed or implied, or assumes any legal liability or responsibility for the accuracy, completeness, or usefulness of any information, apparatus, product, or process disclosed, or represents that its use would not infringe privately owned rights. Reference herein to any specific commercial product, process, or service by trade name, trademark, manufacturer or otherwise does not necessarily constitute or imply its endorsement, recommendation, or favoring by the United States government or Lawrence Livermore National Security, LLC. The views and opinions of authors expressed herein do not necessarily state or reflect those of the United States government or Lawrence Livermore National Security, LLC, and shall not be used for advertising or product endorsement purposes LLNL-JRNL-776860.

*Corresponding author.
schlossberg1@llnl.gov

[1] O. A. Hurricane, D. A. Callahan, D. T. Casey, P. M. Celliers, C. Cerjan, E. L. Dewald *et al.*, Fuel gain exceeding unity in an inertially confined fusion implosio, Nature (London) **506**, 343 (2014).
[2] C. K. Li, F. H. Séguin, J. A. Frenje, R. D. Petrasso, J. A. Delettrez, P. W. McKenty *et al.*, Effects of Nonuniform Illumination on Implosion Asymmetry in Direct-Drive Inertial Confinement Fusion, Phys. Rev. Lett. **92**, 205001 (2004).
[3] M. Gatu Johnson, J. P. Knauer, C. J. Cerjan, M. J. Eckart, G. P. Grim, E. P. Hartouni *et al.*, Indications of flow near maximum compression in layered deuterium-tritium implosions at the National Ignition Facility, Phys. Rev. E **94**, 021202(R) (2016).
[4] M. Gatu Johnson, B. D. Appelbe, J. P. Chittenden, J. Delettrez, C. Forrest, J. A. Frenje *et al.*, Impact of asymmetries on fuel performance in inertial confinement fusion, Phys. Rev. E **98**, 051201(R) (2018).
[5] B. K. Spears, M. J. Edwards, S. Hatchett, J. Kilkenny, J. Knauer, A. Kritcher *et al.*, Mode 1 drive asymmetry in inertial confinement fusion implosions on the National Ignition Facility, Phys. Plasmas **21**, 042702 (2014).
[6] G. A. Kyrala, J. L. Kline, S. Dixit, S. Glenzer, D. Kalantar, D. Bradley *et al.*, Symmetry tuning for ignition capsules via the symcap technique, Phys. Plasmas **18**, 056307 (2011).
[7] D. Eder, B. Spears, D. Casey, A. Pak, T. Ma, N. Izumi *et al.*, Simulations of symcap and layered NIF experiments with top/bottom laser asymmetry to impose P1 drive on capsules, J. Phys. Conf. Ser. **717**, 012014 (2016).
[8] M. Gatu Johnson, D. T. Casey, J. A. Frenje, C.-K. Li, F. H. Séguin, R. D. Petrasso *et al.*, Measurements of collective fuel velocities in deuterium-tritium exploding pusher and cryogenically layered deuterium-tritium implosions on the NIF, Phys. Plasmas **20**, 042707 (2013).
[9] C. R. Christensen, D. C. Wilson, C. W. Barnes, G. P. Grim, G. L. Morgan, M. D. Wilke, F. J. Marshall, V. Yu. Glebov, and C. Stoeckl, The influence of asymmetry on mix in direct-drive inertial confinement fusion experiments, Phys. Plasmas **11**, 2771 (2004).
[10] A. Pak, L. Divol, C. R. Weber, L. F. Berzak Hopkins, D. S. Clark, E. L. Dewald *et al.*, Impact of Localized Radiative Loss on Inertial Confinement Fusion Implosions, Phys. Rev. Lett. **124**, 145001 (2020).
[11] L. A. Pickworth, B. A. Hammel, V. A. Smalyuk, H. F. Robey, R. Tommasini, L. R. Benedetti *et al.*, Development of new platforms for hydrodynamic instability and asymmetry measurements in deceleration phase of indirectly driven implosions on NIF, Phys. Plasmas **25**, 082705 (2018).
[12] D. T. Casey, B. J. MacGowan, J. D. Sater, A. B. Zylstra, O. L. Landen, J. Milovich *et al.*, Evidence of Three-Dimensional Asymmetries Seeded by High-Density Carbon-Ablator Nonuniformity in Experiments at the National Ignition Facility, Phys. Rev. Lett. **126**, 025002 (2021).
[13] O. L. Landen, D. T. Casey, J-M DiNicola, T. Doeppner, E. P. Hartouni, D. E. Hinkel *et al.*, Yield and compression trends and reproducibility at NIF, High Energy Density Phys. **36**, 100755 (2020).
[14] D. S. Clark, C. R. Weber, A. L. Kritcher, J. L. Milovich, P. K. Patel, S. W. Haan *et al.*, Three-dimensional modeling and hydrodynamic scaling of National Ignition Facility implosions, Phys. Plasmas **26**, 050601 (2019).
[15] D. H. Munro, J. E. Field, R. Hatarik, J. L. Peterson, E. P. Hartouni, B. K. Spears, and J. D. Kilkenny, Impact of temperaure-velocity distribution on fusion neutron peak shape, Phys. Plasmas **24**, 056301 (2017).
[16] B. Appelbe and J. Chittenden, The production spectrum in fusion plasmas, Plasma Phys. Controlled Fusion **53**, 045002 (2011).
[17] T. J. Murphy, The effect of turbulent kinetic energy on inferred temperature from neutron spectra, Phys. Plasmas **21**, 072701 (2014).
[18] L. Berzak Hopkins, L. Divol, C. Weber, S. Le Pape, N. B. Meezan, J. S. Ross *et al.*, Increasing stagnation pressure and thermonuclear performance of inertial confinement fusion capsules by the introduction of a high-Z dopan, Phys. Plasmas **25**, 080706 (2018).
[19] D. D.-M. Ho, S. W. Haan, J. D. Salmonson, D. S. Clark, J. D. Lindl, J. L. Milovich, C. A. Thomas, L. F. Berzak Hopkins, and N. B. Meezan, Implosion configurations for robust ignition using high- density carbon (diamond) ablator for indirect-drive ICF at the National Ignition Facility, J. Phys. **717**, 012023 (2016).
[20] K. L. Baker, C. A. Thomas, D. T. Casey, S. Khan, B. K. Spears, R. Nora *et al.*, High-Performance Indirect-Drive Cryogenic Implosions at High Adiabat on the National Ignition Facility, Phys. Rev. Lett. **121**, 135001 (2018).
[21] D. T. Casey, C. A. Thomas, K. L. Baker, B. K. Spears, M. Hohenberger, S. F. Khan *et al.*, The high velocity, high adiabat, "Bigfoot" campaign and tests of indirect-drive implosion scaling, Phys. Plasmas **25**, 056308 (2018).
[22] V. Yu. Glebov, T. C. Sangster, C. Stoeckl, J. P. Knauer, W. Theobald, K. L. Marshall *et al.*, , Rev. Sci. Instrum. **81**, 10D325 (2010).
[23] R. Hatarik, D. B. Sayre, J. A. Caggiano, T. Phillips, M. J. Eckart, E. J. Bond *et al.*, The National Ignition Facility neutron time-of-flight system and its initial performance (invited), J. Appl. Phys. **118**, 184502 (2015).
[24] R. Hatarik, R. C. Nora, B. K. Spears, M. J. Eckart, G. P. Grim, E. P. Hartouni, A. S. Moore, and D. J. Schlossberg, Using multiple neutron time of flight detectors to determine the hot spot velocity, Rev. Sci. Instrum. **89**, 10I138 (2018).
[25] H. Brysk, Fusion neutron energies and spectra, Plasma Phys. **15**, 611 (1973).
[26] B. Appelbe and J. Chittenden, Relativistically correct DD and DT neutron spectra, High Energy Density Phys. **11**, 30 (2014).
[27] D. H. Munro, Interpreting inertial fusion neutron spectra, Nucl. Fusion **56**, 036001 (2016).
[28] C. B. Yeamans and D. L. Bleuel, The spatially distributed neutron activation diagnostic FNADs at the national ignition facility, Fusion Sci. Technol. **72**, 120 (2017).
[29] A. Pavlik, G. Winkler, H. Vonach, A. Paulsen, and H. Liskien, Precise measurement of cross sections for the 90Zr(n,2n)89Zr reaction from threshold to 20 MeV, J. Phys. G **8**, 1283 (1982).
[30] J. D. Kilkenny, J. A. Caggiano, R. Hatarik, J. P. Knauer, D. B. Sayre, B. K. Spears *et al.*, Understanding the stagnation and burn of implosions on NIF, J. Phys. **688**, 012048 (2016).

[31] H. G. Rinderknecht, R. Bionta, G. Grim, R. Hatarik, H. Khater, D. Schlossberg, and C. Yeamans, Velocity correction for neutron activation diagnostics at the NIF, Rev. Sci. Instrum. **89**, 10I125 (2018).
[32] P. M. Bell, D. K. Bradley, J. D. Kilkenny, A. Conder, C. Cerjan, C. Hagmann *et al.*, Radiation hardening of gated x-ray imagers for the National Ignition Facility (invited), Rev. Sci. Instrum. **81**, 10E540 (2010).
[33] L. R. Benedetti, P. M. Bell, D. K. Bradley, C. G. Brown, S. M. Glenn, R. Heeter *et al.*, Crosstalk in x-ray framing cameras: Effect on voltage, gain, and timing (invited), Rev. Sci. Instrum. **83**, 10E135 (2012).
[34] D. B. Ress, R. A. Lerche, R. J. Ellis, S. M. Lane, and K. A. Nugent, Neutron imaging of laser fusion targets, Science **241**, 956 (1988).
[35] G. P. Grim, C. W. Barnes, P. A. Bradley, C. R. Christensen, A. Hauer, G. L. Morgan *et al.*, Neutron Imaging at the NIF, J. Phys. IV (France) **133**, 913 (2006).
[36] P. Volegov, C. R. Danly, D. N. Fittinghoff, G. P. Grim, N. Guler, N. Izumi *et al.*, Neutron source reconstruction from pinhole imaging at National Ignition Facility, Rev. Sci. Instrum. **85**, 023508 (2014).
[37] C. V. Young, L. Masse, D. T. Casey, B. J. MacGowan, O. L. Landen, D. A. Callahan, N. B. Meezan, R. Nora, and P. K. Patel, View factor estimation of hot spot velocities in inertial confinement fusion implosions at the National Ignition Facility, Phys. Plasmas **27**, 082702 (2020).
[38] L. A. Pickworth, B. A. Hammel, V. A. Smalyuk, H. F. Robey, L. R. Benedetti, L. Berzak Hopkins *et al.*, Visualizing deceleration-phase instabilities in inertial confinement fusion implosions using an "enhanced self-emission" technique at the National Ignition Facility, Phys. Plasmas **25**, 054502 (2018).
[39] M. M. Marinak, G. D. Kerbel, N. A. Gentile, O. Jones, D. Munro, S. Pollaine, T. R. Dittrich, and S. W. Haan, Three-dimensional HYDRA simulations of National Ignition Facility targets, Phys. Plasmas **8**, 2275 (2001).
[40] See Supplemental Material at http://link.aps.org/supplemental/10.1103/PhysRevLett.127.125001 for detailed HYDRA simulations and explicit fit functions to the data shown.
[41] B. J. MacGowan, O. L. Landen, D. T. Casey, C. Young, D. A. Callahan, E. P. Hartouni *et al.*, Trending low mode asymmetries in NIF capsule drive using a simple viewfactor metric, High Energy Density Phys. **40**, 100944 (2021).
[42] O. A. Hurricane, D. T. Casey, O. Landen, A. L. Kritcher, R. Nora, P. K. Patel *et al.*, An analytic asymmetric-piston model for the impact of mode-1 shell asymmetry on ICF implosions, Phys. Plasmas **27**, 062704 (2020).
[43] D. T. Casey, O. L. Landen, E. Hartouni, R. M. Bionta, K. D. Hahn, P. L. Volegov *et al.*, Three dimensional low-mode areal-density non-uniformities in indirect-drive implosions at the National Ignition Facility, Phys. Plasmas **28**, 042708 (2021).
[44] L. C. Jarrott, B. Bachmann, T. Ma, L. R. Benedetti, J. E. Field, E. P. Hartouni *et al.*, Thermal Temperature Measurements of Inertial Fusion Implosions, Phys. Rev. Lett. **121**, 085001 (2018).
[45] J. D. Kilkenny, P. Bell, R. Hanks, G. Power, R. E. Turner, and J. Wiedwald, High-speed gated x-ray imagers (invited), Rev. Sci. Instrum. **59**, 1793 (1988).
[46] S. M. Glenn, L. R. Benedetti, D. K. Bradley, B. A. Hammel, N. Izumi, S. F. Khan *et al.*, Extracting core shape from x-ray images at the National Ignition Facility, Rev. Sci. Instrum. **83**, 10E519 (2012).
[47] S. F. Khan, N. Izumi, S. Glenn, R. Tommasini, L. R. Benedetti, T. Ma *et al.*, Automated analysis of hot spot X-ray images at the National Ignition Facility, Rev. Sci. Instrum. **87**, 11E334 (2016).
[48] T. R. Dittrich, O. A. Hurricane, L. F. Berzak-Hopkins, D. A. Callahan, D. T. Casey, D. Clark *et al.*, Simulations of fill tube effects on the implosion of high-foot NIF ignition capsules, J. Phys. Conf. Ser. **717**, 012013 (2016).
[49] C. R. Weber, D. S. Clark, A. Pak, N. Alfonso, B. Bachmann, L. F. Berzak Hopkins *et al.*, Mixing in ICF implosions on the National Ignition Facility caused by the fill-tube, Phys. Plasmas **27**, 032703 (2020).
[50] K. L. Baker, C. A. Thomas, T. R. Dittrich, O. Landen, G. Kyrala, D. T. Casey *et al.*, Fill tube dynamics in inertial confinement fusion implosions with high density carbon ablators, Phys. Plasmas **27**, 112706 (2020).
[51] J. J. Ruby, A. Pak, J. E. Field, T. Ma, B. K. Spears, L. R. Benedetti *et al.*, Spatially resolved X-ray emission measurements of the residual velocity during the stagnation phase of inertial confinement fusion implosion experiments, Phys. Plasmas **23**, 072701 (2016).
[52] H. W. Herrmann, N. Hoffman, D. C. Wilson, W. Stoeffl, L. Dauffy, Y. H. Kim *et al.*, Diagnosing inertial confinement fusion gamma ray physics (invited), Rev. Sci. Instrum. **81**, 10D333 (2010).
[53] V. A. Thomas and R. J. Kares, Drive Asymmetry and the Origin of Turbulence in an ICF Implosion, Phys. Rev. Lett. **109**, 075004 (2012).

Supplemental Material for:

"Observation of hydrodynamic flows in imploding fusion plasmas on the National Ignition Facility"

D.J. Schlossberg[1], G.P. Grim[1], D.T. Casey[1], A.S. Moore[1], R. Nora[1], B. Bachmann[1], L.R. Benedetti[1], R.M. Bionta[1], M.J. Eckart[1], J.E. Field[1], D.N. Fittinghoff[1], M. Gatu Johnson[2], V. Geppert-Kleinrath[3], E.P. Hartouni[1], R. Hatarik[1], W.W. Hsing[1], L.C. Jarrott[1], S.F. Khan[1], J.D. Kilkenny[4], O.L. Landen[1], B.J. MacGowan[1], A.J. Mackinnon[1], K.D. Meaney[3], D.H. Munro[1], S.R. Nagel[1], A. Pak[1], P.K. Patel[1], B.K. Spears[1], P.L. Volegov[3], and C.V. Young[1]

[1]*Lawrence Livermore National Laboratory, Livermore, California 94550, USA*
[2]*Massachusetts Institute of Technology Plasma Science and Fusion Center, Cambridge, Massachusetts 02139, USA*
[3]*Los Alamos National Laboratory, Los Alamos, New Mexico 87544, USA*
[4]*General Atomics, La Jolla, California 92121, USA*

Table of Contents

LLNL-JRNL-824784

Relevance of yield scaling with v_{HS} to ignition-type implosions

In this manuscript, the effect of hot-spot drift velocity (v_{HS}) on performance of gas-filled implosions is explored in detail. These effects are directly relevant to ignition targets, as can be seen in the figure below. Here the DT neutron yield is plotted as a function of hot spot drift speed. The stars mark the same implosions as in the main article, and a fit is applied of the form $y = C_0 \cdot (1 - C_1 x^2)$.

Additionally, the majority of DT ice-layer (i.e. ignition-type) targets shot on NIF since 2017 are shown as grey squares. Their yield has been reduced by a factor of 10x but no further processing has been done. There is a clear maximum boundary along the fit to the gas-filled targets presented here. Most of the shots lie below this boundary, since for complex, sensitive ignition targets there are often more degradations than solely asymmetric drive. In fact, it is for just this reason that gas-filled targets were chosen for this campaign, in order to provide simplified, clear, quantitative evidence of the effects of drive asymmetry on implosion performance.

Additionally, a model developed by Hurricane *et al.* has been applied and is shown in blue. The model was developed for ignition targets, and it also lies near the boundary of both the gas-filled and ice-layer targets.

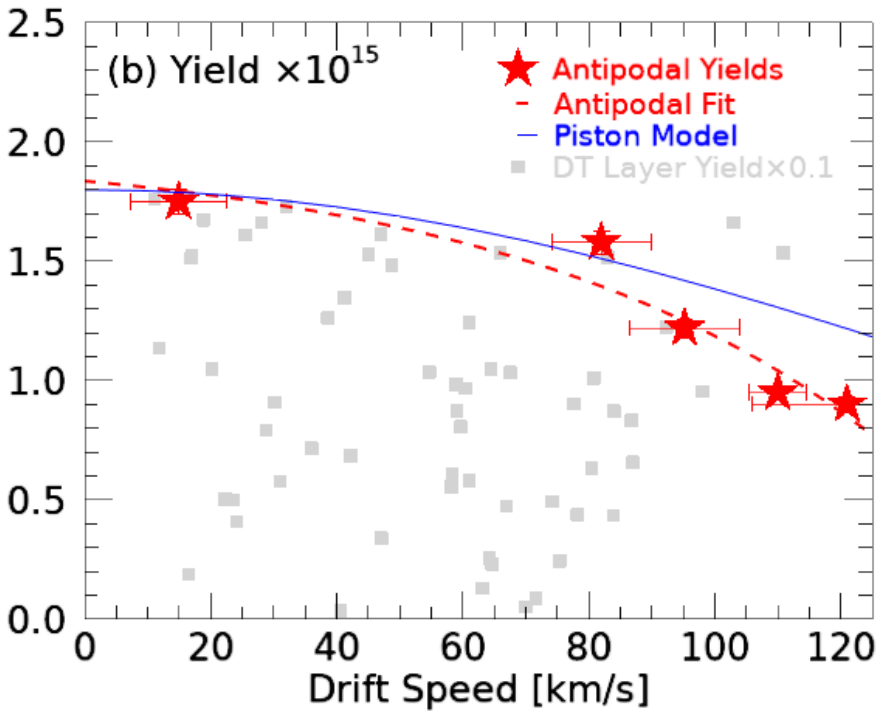

Time-resolved, 2D HYDRA simulations suggest vortical flows

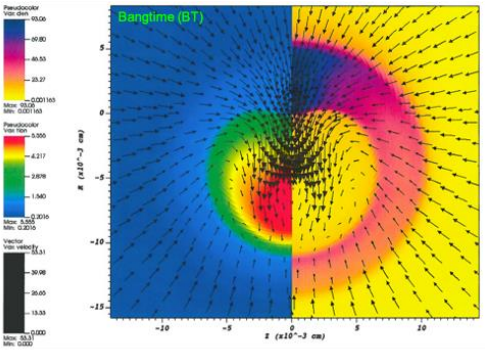

Time-sequence of 2D HYDRA simulations, with 5% P1/P0 applied x-ray drive asymmetry in the downward direction.

Black arrows = velocity vectors; length ∝ magnitude
Left side = pseudo color image of ion density
Right side = pseudo color image of ion temperature

A region of interest (ROI) where retrograde flows are observed is between [5, 10] on the horizontal axis and [-10, -5] on the vertical axis.

At bangtime (BT), most flow fields in the ROI are directed radially inward.

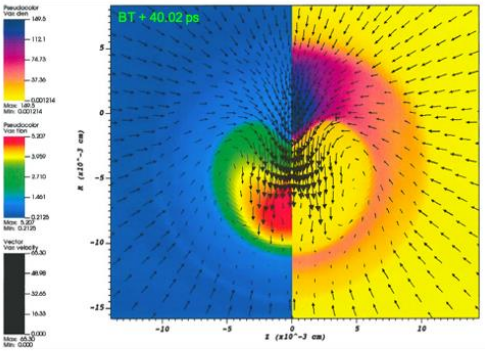

At BT + 40.02 ps, there is slight perturbation of flow direction in the ROI, where vectors point slightly more upward.

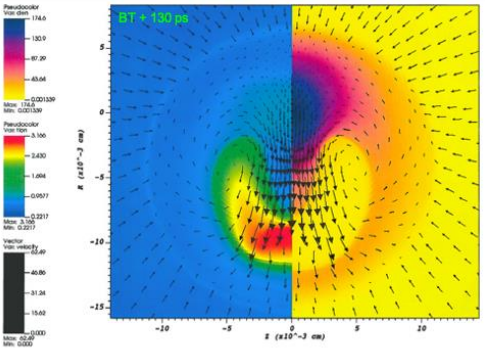

At BT + 130 ps, flows in the region of interest have changed direction by ≥ 90°. Following streamlines, it is evident that flows are moving downward in the center, around and outward near the bottom of the capsule, and upward along the outer edge.

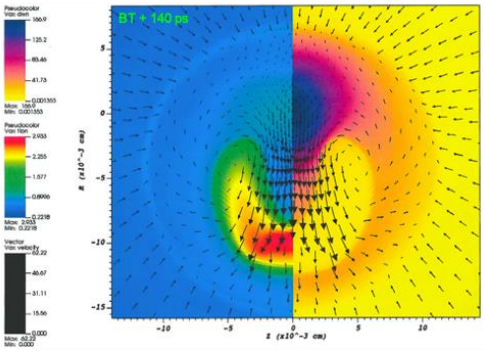

At BT + 140 ps (the last available simulation image), the vortical flow pattern persists.

Throughout all images, there is increasing T_{ion} along the direction parallel to $\vec{v}_{HS}$, and increasing n_{ion} antiparallel to this direction. These localized increases are consistent with the increased limb brightening seen in x-ray images in Figure 3 of the main article.

Measured and synthetic x-ray and neutron images show similar features

Experimental data from N171120-001-999 is shown, which had an induced P1/P0 drive of 3.7%.
Synthetic data from 2D HYDRA simulation using 3.75% P1/P0 asymmetric drive.

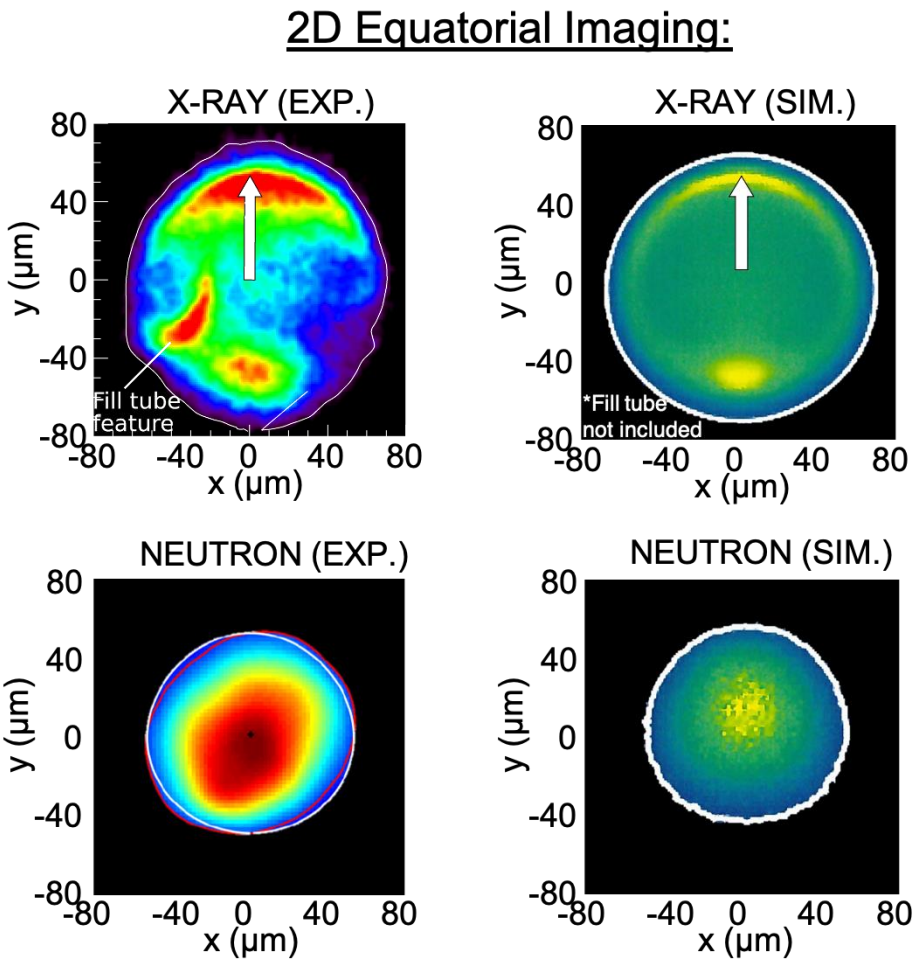

Peak neutron production occurs at roughly 0.66 × R_{HS}

The neutron images shown above and in the main manuscript map the three-dimensional, approximately spherical hotspot onto a necessarily two-dimensional detector. This means the intensity at each pixel in the neutron image is the line-integral of that sightline through the hot spot. Since the hot spot is spherical, the central chords pass through the "thickest" portion of the hot spot and are hence the largest; however, this does not dictate that peak neutron production is centered in the hot spot. This is important to understand the relative contribution of retrograde flows in the outer half of the hot spot radius (as shown above) to the apparent ion temperature.

Peak neutron production depends on the hot spot's density and temperature profiles, $n(R)$ and $T_{DT}^{thermal}$. Additionally, for the spherical geometry of these implosions the outer radii are weighted more strongly due to larger volume per ∂r. This generally places peak neutron production from $\sim 0.60 \leq R \leq 0.70$. This has been verified experimentally as well as analytically.

A 3D volumetric reconstruction [P.L. Volegov, *et al.*, J. Applied Physics **122**, 175901 (2017)] was calculated based on the measured neutron images for one implosion in this series. On N181211-001-999, shown in the manuscript in Fig. 3 third column with $P1/P0 = +2.0\%$, neutron images along three nearly-orthogonal lines-of-sight were obtained. Neutron yield as a function of radius was calculated from this reconstruction and the rate of neutron production was calculated from the derivative of this function. These are shown below. Peak neutron production is quite far from centrally located (R=0) and occurs at roughly $0.66P_0$, where P_0 = 48.4±7.2 μm for this shot.

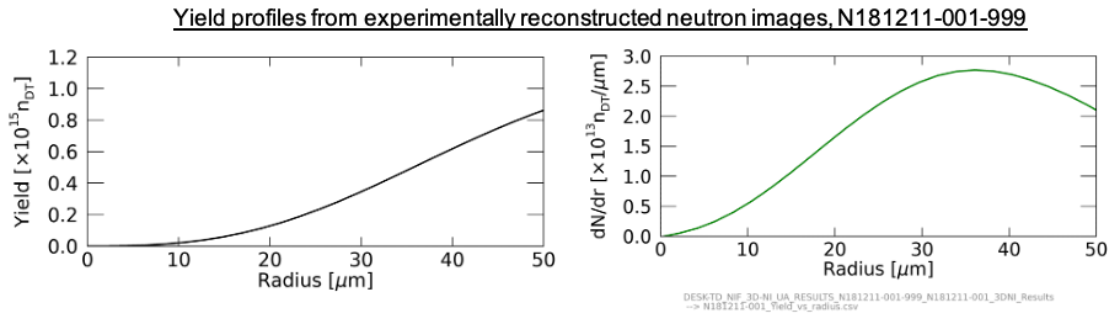

Additionally, analytic expressions for neutron production as a function of radius have been given in the literature [e.g., P.K. Patel, *et al.*, Phys. Plasmas **27**, 050901 (2020), Eq. (5-7)]. Commonly an adiabatic temperature profile is assumed for the hot spot, and a density profile is then derived using the ideal gas law. Using experimentally measured parameters from N181211-001-999 and N171022-002-999, the resultant yields/radius vs radius are shown below. For N181211-001, this agrees well with the measured profile with peak production at $0.65P_0$.

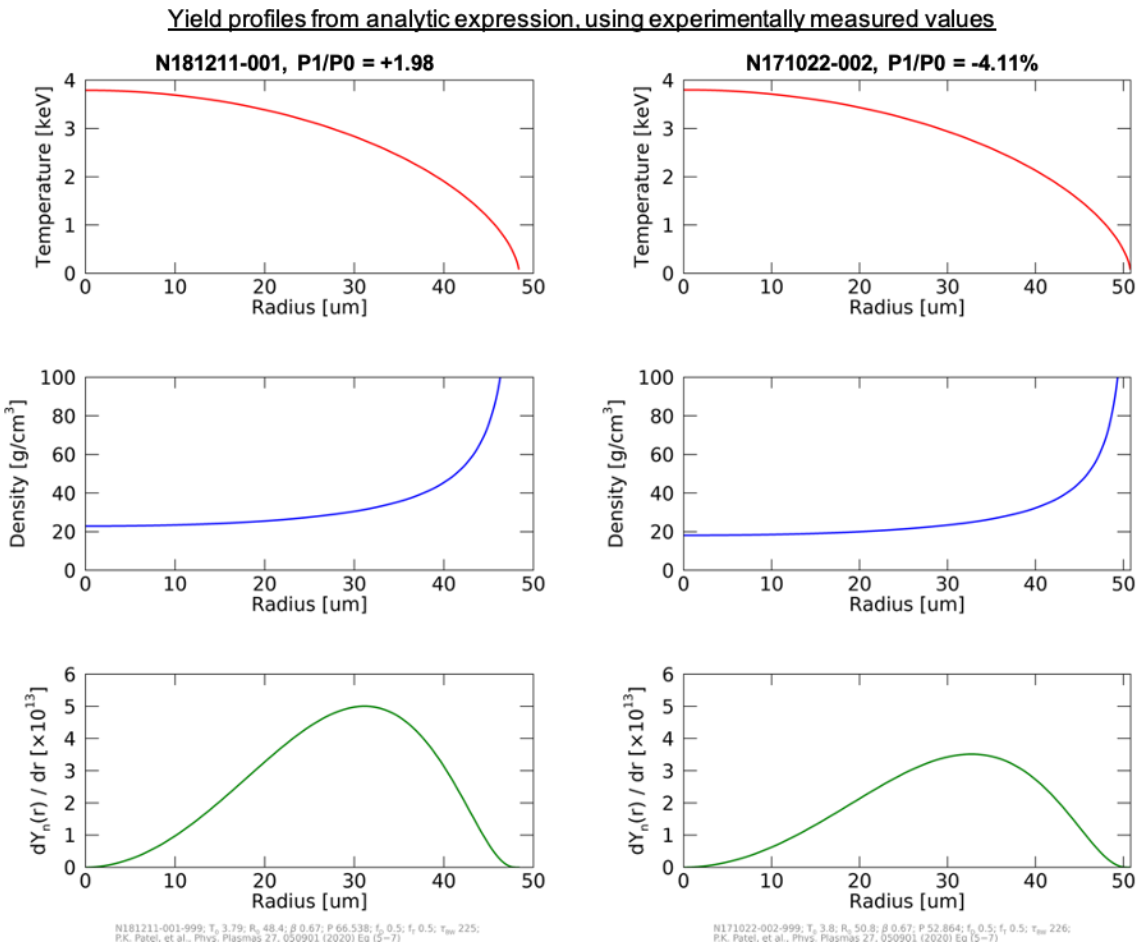

For the case of N171022-002, $Y_n(R > 30\mu m) \approx Y_n(R < 30\mu m)$. The simulated flow fields shown in the manuscript and above for $P1/P0 = 5\%$ most nearly correspond to N171022's induced 4% P1/P0. Notably, the simulated retrograde flow fields occupy the outer half of the hot spot radius. Since roughly half the total yield is produced in this region, it's suggestive that these flows significantly contribute to the observed broadening of T_{ion}^{app}.

Explicit fit functions used in Figure 4 are defined

For reference, the fits presented in the manuscript are shown below with their definitions:

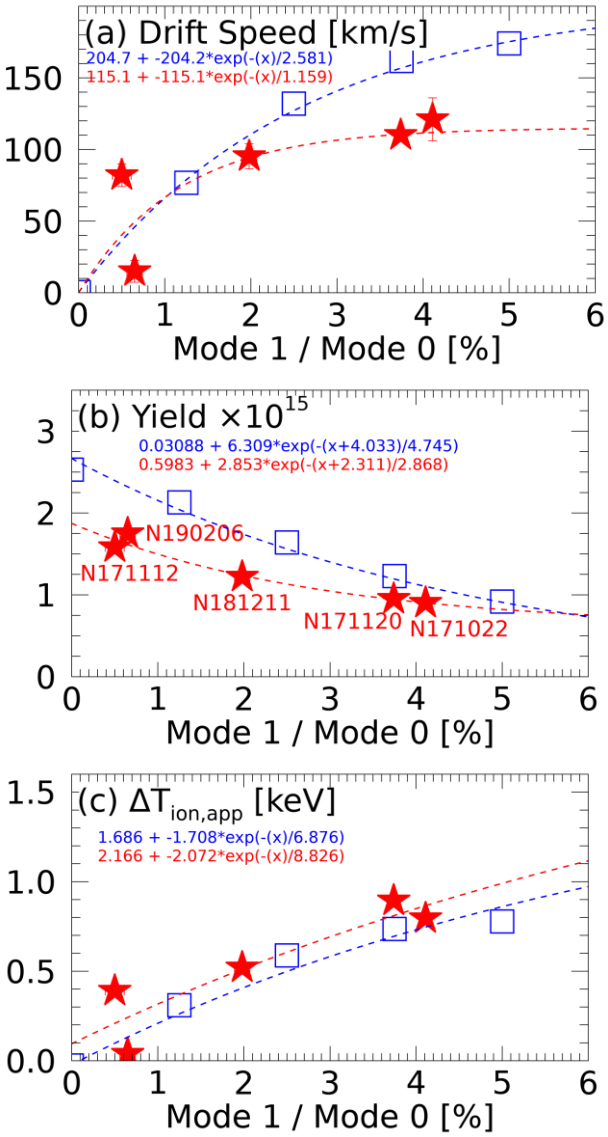

NIF shot numbers are given for data shown in all figures

This work focused on five NIF shots with varying levels of induced drive asymmetry:

N171022-002-999
N171112-002-999
N171120-001-999
N181211-001-999
N190206-002-999

These shots appear as noted below in the following figures:

Figure 1:
(c) -P1 drive = N171022-002-999
Balanced = N171112-002-999

Figure 2:
N171022-002-999

Figure 3:
From left to right:
$\frac{P1}{P0} = -4.1\%$: N171022-002-999
$\frac{P1}{P0} = +0.6\%$: N190206-002-999
$\frac{P1}{P0} = +2.0\%$: N181211-001-999
$\frac{P1}{P0} = +3.7\%$: N171120-001-999

Top row is time-integrated, penumbral x-ray imaging from the "DIXI" line-of-sight (90°, 100°).
Bottom row is time-integrated x-ray imaging from the "NIS-1" line-of-sight (90°, 315°). Overlaid are contours of primary neutron production from the same LoS.

Figure 4:
As shown in part (b)

Figure 5:
-P1 N171022-002-999
+P1 N171120-001-999
~+P1 N181211-001-999
Bal. N190206-002-999

Figure 6:

Plot Label	P1/P0 [%]	NIF Shot Number
-P1	4.1 ± 0.1	N171022-002-999
+P1	3.7 ± 0.1	N171120-001-999
Bal.	0.6 ± 0.1	N190206-002-999

Table 1

Implosion parameters for shots of interest, trending with P1/P0

From left to right columns decrease in inferred $|P1/P0|$.
Quantities in rows are grouped by type (e.g., yield, ion temperature, etc.).

Parameter	**Units**	**N171022-002**	**N171120-001**	**N181211-001**	**N190206-002**	**N171112-002**
Inferred P1/P0	%	-4.11 ±0.07	3.74 ±0.07	1.98 ±0.09	0.65 ±0.09	0.50 ±0.11
Hot Spot Velocity						
v_{HS}, magnitude	km/s	121 ±15	118 ±16	78 ±20	15 ±22	86 ±30
v_{HS}, polar angle	°	177 ±14	8 ±12	24 ±22	95 ±70	115 ±20
v_{HS}, azimuth	°	171 ±168	356 ±95	243 ±43	155 ±89	47 ±18
Neutron Yield						
Y_n (13-15 MeV)	$\times 10^{15}$	0.90 ±0.03	0.95 ±0.03	1.22 ±0.38	1.71 ±0.46	1.58 ±0.05
Y_n (2.2-2.7 MeV)	$\times 10^{12}$	3.66 ±0.14	3.54 ±0.17	4.58 ±0.18	6.29 ±0.29	5.97 ±0.32
Ion Temperature						
T_{DT}^{app}, average	keV	4.27 ±0.18	4.24 ±0.20	4.19 ±0.12	4.10 ±0.12	4.08 ±0.12
ΔT_{DT}^{app}	keV	0.9 ±0.1	1.0 ±0.1	0.5 ±0.1	0.0 ±0.1	0.3 ±0.1
T_{DD}^{app}, minimum	keV	3.80 ±0.27	3.78 ±0.27	3.79 ±0.27	3.61 ±0.27	3.81 ±0.27
Bangtime						
Bangtime (γ)	ns	7.13 ±0.03	7.09 ±0.03	7.17 ±0.03	7.17 ±0.1	7.17 ±0.03
Bangtime (x-ray)	ns	7.14	7.11			7.17
Burnwidth						
Burnwidth (γ)	ps	226 ±30	235 ±30	225 ±18		223 ±30
Burnwidth (x-ray)	ps	192	182			194
Shape (CNXI)						
P0 (nuclear)	μm	50.8 ±6.7	56.5 ±7.6	48.4 ±7.2	40.0 ±5.0	44.9 ±5.8
P0 (x-ray)	μm	69.5 ±1.5	68.4 ±1.5	68.3 ±0.1	59.3 ±1.3	61.7 ±1.3

Table 2

Discussion of anomalous drift speed for N171112-002

In addition to mode 1 asymmetries induced by laser imbalance, recent work has also shown that uneven thickness around the ablator shell can induce mode 1 asymmetries and subsequent hot-spot velocities [D.T. Casey, *et al.*, Phys. Rev. Lett. **126** 025002 (2021); D.T. Casey, *et al.*, Phys. Plasmas **28** 042708 (2021)]. The implosions presented in this work were conducted prior to the recent increase in metrology and documentation of these thickness variations. Nevertheless, analysis has been done on the data for the 5 shells used in this study. Extrapolations from the recorded viewing angle have identified the potential for 0.37% P1/P0 drive in three capsules. If N1711112 was affected by this additional P1 source, the discrepancies in Figure 4 a-c would be lessened if not resolved.

Disclaimer